ACS Catalysis

Research Article

pubs.acs.org/acscatalysis

Reduction of Nitric Oxide with Hydrogen on Catalysts of Singly Dispersed Bimetallic Sites Pt_1Co_m and Pd_1Co_n

Luan Nguyen,[†,∥] Shiran Zhang,[†,∥] Lei Wang,[§] Yuanyuan Li,[⊥] Hideto Yoshida,[¶] Anitha Patlolla,[⊥] Seiji Takeda,[¶] Anatoly I. Frenkel,[*,⊥] and Franklin (Feng) Tao[*,†]

[†]Department of Chemical and Petroleum Engineering and Department of Chemistry, University of Kansas, Lawrence, Kansas 66045, United States

[§]Institute of Process Engineering, Chinese Academy of Sciences, Beijing 100190, China

[⊥]Department of Physics, Yeshiva University, New York, New York 10016, United States

[¶]Institute of Scientific and Industrial Research, Osaka University, Osaka 567-0047, Japan

Supporting Information

ABSTRACT: The bimetallic catalyst has been one of the main categories of heterogeneous catalysts for chemical production and energy transformation. Isolation of the continuously packed bimetallic sites of a bimetallic catalyst forms singly dispersed bimetallic sites which have distinctly different chemical environment and electronic state and thus exhibit a different catalytic performance. Two types of catalysts consisting of singly dispersed bimetallic sites Pt_1Co_m or Pd_1Co_n (m and n are the average coordination numbers of Co to a Pt or Pd atom) were prepared through a deposition or impregnation with a following controlled calcination and reduction to form Pt_1Co_m or Pd_1Co_n sites. These bimetallic sites are separately anchored on a nonmetallic support. Each site only consists of a few metal atoms. Single dispersions of these isolated bimetallic sites were identified with scanning transmission electron microscopy. Extended X-ray absorption fine structure spectroscopy (EXAFS) revealed the chemical bonding of single atom Pt_1 (or Pd_1) to Co atoms and thus confirmed the formation of bimetallic sites, Pt_1Co_m and Pd_1Co_n. Reduction of NO with H_2 was used as a probing reaction to test the catalytic performance on this type of catalyst. Selectivity in reducing nitric oxide to N_2 on Pt_1Co_m at 150 °C is 98%. Pd_1Co_n is active for reduction of NO with a selectivity of 98% at 250 °C. In situ studies of surface chemistry with ambient-pressure X-ray photoelectron spectroscopy and coordination environment of Pt and Pd atoms with EXAFS showed that chemical state and coordination environment of Pt_1Co_m and Pd_1Co_n remain during catalysis up to 250 and 300 °C, respectively. The correlation of surface chemistries and structures of these catalysts with their corresponding catalytic activities and selectivities suggests a method to develop new bimetallic catalysts and a new type of single site catalysts.

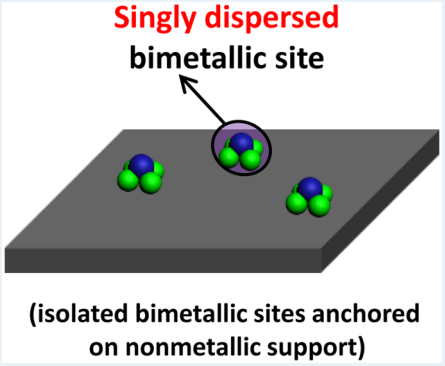

KEYWORDS: *single site catalysis, bimetallic, AP-XPS, EXAFS, in-situ and operando*

1. INTRODUCTION

The bimetallic catalyst is one of the main categories of heterogeneous catalysts for chemical and energy transformations. On the surface of a bimetallic catalyst nanoparticle, catalytic sites are continuously packed. One type of bimetallic sites consists of a metal atom M with one or more metal atoms A bonding to the metal atom M, which forms a site M_1A_a ($a \geq 1$). Compared to the continuous distribution of bimetallic sites on the surface of a bimetallic nanoparticle (Figure 1a), bimetallic sites M_1A_a could be separately anchored on a nonmetallic substrate (Figure 1b). From an electronic state point of view, an isolated bimetallic site M_1A_n anchored on a nonmetallic substrate is expected to exhibit a cationic state instead of a metallic state of these continuously dispersed bimetallic sites on the surface of a bimetallic nanoparticle (Figure 1a). Compared to continuously packed bimetallic sites on the surface of a bimetallic nanoparticle, an isolated bimetallic site M_1A_a (Figure 1b) supported on a nonmetallic oxide surface could exhibit a quite different catalytic performance due to their different electronic states.

Preparation of a catalyst consisting of single atom sites can be done by deposition of a very small amount of guest metal to a substrate metal. The anchored single guest atoms were visualized with scanning tunneling microscopy (STM). For instance, a low coverage of Pd atoms was added to the surface of Au substrate and thus formed Pd monomers;[1] the separation of continuous Pd sites by Au atoms can inhibit the formation of undesirable products. In addition, a small number of Au atoms were deposited to the surface of Ni(111) and thus formed singly dispersed Au atoms on the Ni(111) surface; the single

Received: April 22, 2015
Revised: November 20, 2015

DOI: 10.1021/acscatal.5b00842
ACS Catal. 2016, 6, 840−850

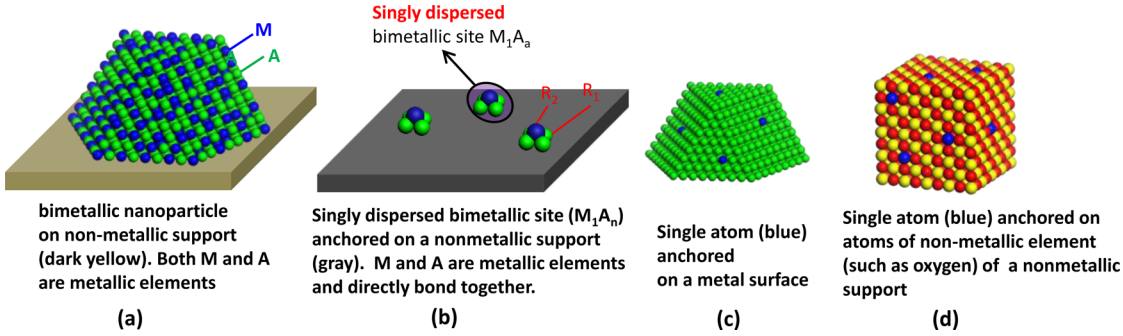

Figure 1. Schematics of (a) M−A bimetallic nanoparticle consisting of continuously dispersed bimetallic sites, (b) catalyst consisting of isolated bimetallic sites M_1A_a anchored on a nonmetallic support, (c) a metal particle A anchored with single atoms M, and (d) single atom (blue) of a metallic element bonded to atoms of nonmetallic elements of a nonmetallic support. Blue (M) and green (A): atoms of metallic elements. Although these schematics are shown in packings at the atomic level, the positions of atoms in the schematics do not mean the actual positions in catalysts.

atoms of Au largely tuned the electronic state of Ni atoms through electron transfer from Au 5d to Ni atom. This charge transfer decreases the adsorption energy of carbon atoms on Ni(111) and thus inhibits the formation of coke layers on a Ni catalyst.[2] Recently, Sykes et al. anchored guest metal atoms Pd to Cu(111) to form a new type of single atom catalysts exhibiting quite high selectivity for hydrogenation.[3] Other than anchoring metal atoms on the surface of a metal support,[1−3] metal atoms have been introduced to the surface of an oxide to bond with oxygen atoms. For example, metal atoms were anchored to the internal surface of nanopores of zeolite (Cu or Ni/ZSM-5),[4−8] to the defective surface of graphene (Pt_1/graphene),[9,10] and to oxygen atoms of surface of FeO_x (Pt/FeO_x).[11,12]

It is noted that a catalyst consisting of singly dispersed bimetallic sites (Figure 1b) is different from the other two types of single atom catalysts (Figure 1c,d). This is because the M atom of a singly dispersed bimetallic site M_1A_n directly bonds with another metal atom (A)[13] instead of only binding to atoms of nonmetallic elements such as oxygen atoms of an oxide support (Figure 1d).[11] In addition, a singly dispersed bimetallic site[13] is different from the single atoms M anchored on surface of a substrate metal A[3], as shown in Figure 1c. To prepare a catalyst consisting of singly dispersed bimetallic sites, a straightforward method could be a deposition of organometallic molecules consisting of M−A bonds. Unfortunately, there are few molecular precursors which consist of M−A bonds.

Here we used a method termed deposition−calcination−reduction[13] to prepare catalysts consisting of singly dispersed bimetallic sites. It begins with a deposition or impregnation of a precursor of guest atoms M to the surface of a reducible oxide A_xO_y, followed by calcination to chemically bond the guest metal atoms M to oxygen atoms of surface of A_xO_y, and it concludes with a controlled reduction to remove oxygen atoms between M and A_xO_y to form the M_1A_n nanocluster anchored on A_xO_y.

We selected Co_3O_4 as a representative transition metal oxide to develop catalysts with the aid of in situ characterization including AP-XPS and EXAFS. DFT calculations showed the energy barrier for hopping oxygen vacancies through releasing oxygen atoms is 0.26 eV.[14] The high mobility of surface oxygen atoms makes Co_3O_4 readily generate surface oxygen vacancies under a mild condition. More importantly, the high mobility of surface lattice oxygen atoms suggests that oxygen atom of Pt−O−Co or Pd−O−Co on the surface of Co_3O_4 could be readily removed by H_2 in the reduction step and thus allow a direct bonding between Pt (or Pd) and Co atoms of Co_3O_4 surface to form bimetallic sites M_1Co_m.

In this work, catalyst precursor, Co_3O_4 with singly dispersed Pt or Pd atoms was prepared as to form catalysts of singly dispersed bimetallic sites. A following reduction in 5% H_2 or a mixture of NO and H_2 formed catalysts of singly dispersed bimetallic sites Pt_1Co_m or Pd_1Co_n. Reduction of nitric oxide with H_2 ($2NO + 2H_2 = N_2 + 2H_2O$)[15−21] was taken as a probing reaction to test catalytic performances of catalysts consisting of singly dispersed bimetallic sites. Our studies showed that these catalysts consisting of singly dispersed bimetallic sites exhibit selectivity of 98−100% for production of N_2 in the temperature range of 150−300 °C. In situ studies of AP-XPS confirmed that Pt and Pd are at a cationic state during catalysis. EXAFS studies showed that singly dispersed bimetallic sites are formed on Co_3O_4, and single dispersion of these bimetallic sites remains during catalysis up to 300 °C. This work demonstrated the development of a new type of bimetallic catalysts in the form of single sites active for different catalytic reactions.

2. EXPERIMENTAL SECTION

Catalyst Synthesis. Synthesis of Co_3O_4 nanorods anchoring Pt or Pd atoms includes three steps: synthesis of Co_3O_4 nanorods, deposition precipitation of Pt or Pd on surface of the Co_3O_4 nanorods, and calcination under a mild condition. Co_3O_4 nanorods were prepared by the calcination of a cobalt hydroxycarbonate precursor obtained by the precipitation of 2.49 g of cobalt acetate (99.995%, Aldrich) with sodium carbonate in 30 mL of ethylene glycol.[22] When cobalt acetate was mixed with ethylene glycol (99.8%, Aldrich) at 160 °C, the $-OCH_2-CH_2O-$ chain was tightly bound with the cobalt cations. The addition of 100 mL of aqueous sodium carbonate solution (0.2 mol/L) at a rate of 1.11 mL/min resulted in the formation of a solid cobalt hydroxycarbonate incorporating ethylene glycol, having a shape of nanorod. A subsequent calcination of the precursor at 350 °C in air for 4 h forms well-crystallized Co_3O_4 nanorods.

Subsequently, 1.5 mg of Pt acetylacetonate (Aldrich), 7.5 mg of Pt acetylacetonate (Aldrich), or 5.7 mg of Pd acetylacetonate (Aldrich) was dissolved in 10 mL of pure ethanol. The solution of precursors was added to 20 mL of ethanol with dispersed 0.3 g of Co_3O_4 nanorods. Vigorous stirring and evaporation of solvent at 45 °C were necessary to make sure a homogeneous impregnation of metal ions on the surface of Co_3O_4 nanorods for the preparation of 0.1 atom % Pt/Co_3O_4, 0.5 atom % Pt/

DOI: 10.1021/acscatal.5b00842
ACS Catal. 2016, 6, 840−850

Co_3O_4, or 0.5 atom % Pd/Co_3O_4. Due to steric effect of the large acetylacetonate group and the low concentration of precursor of Pt or Pd, metal atoms are separately anchored on the Co_3O_4 support. A subsequent calcination in air at 350 °C for 3 h removes the carbon species and anchors metal ions to the surface of Co_3O_4. A further pretreatment in 5% H_2 will be described in the following section.

Catalytic Measurements. Catalysts were mixed with quartz (60−80 meshes) to make up the catalyst bed with a volume of 1 cm^3. They were loaded into a plug-in fixed-bed flow reactor. Nitric oxide, hydrogen, and argon were premixed before introducing them to the reactor. In the mixture of reactant, the pressure ratio of NO to H_2 is 1:1. The mixture was placed into a quartz tube. Blank experiments showed no activity in NO reduction with H_2 in the temperature range of 25−300 °C. Products were analyzed with a gas chromatograph. Conversion of NO was calculated with the equation:

$$X\% = \frac{N_{NO} - N^{T}{}_{NO}}{N_{NO}} \times 100\%$$

Here N^{T}_{NO} is the mole of NO detected at a reaction temperature, T. N_{NO} stands for the moles of NO introduced before catalysis. Selectivity to the production of N_2 was calculated with the equation:

$$S_{N_2}\% = \frac{2N^{T}{}_{N_2}}{N_{NO} - N^{T}{}_{NO}} \times 100\%$$

Here $N^{T}_{N_2}$ is the mole of N_2 detected at a reaction temperature. Selectivity to the production of N_2O was calculated with the equation:

$$S_{N_2O}\% = \frac{2N^{T}{}_{N_2O}}{N_{NO} - N^{T}{}_{NO}} \times 100\%$$

Here $N^{T}_{N_2O}$ is the mole of N_2O detected at a reaction temperature. Because N_2O and NH_3 are the byproducts, the selectivity for the production of NH_3 was calculated with the equation:

$$S_{NH_3}\% = 100\% - S_{N_2}\% - S_{N_2O}\%$$

Ex Situ Characterization of Catalysts. Size, shape, and lattice fringe of pure Co_3O_4, Pt/Co_3O_4, and Pd/Co_3O_4 were characterized with Titan TEM (FEI Titan 80−300, 300 kV FEG TEM with a point resolution of 0.2 nm). High-angle annual dark field-scanning transmission electron microscopy (HAADF-STEM) images were collected on JEOL JEM-ARM 200F with a CEOS probe corrector in Takeda group at Osaka University at Japan. The used accelerating voltage is 200 kV. The HAADF-STEM resolution is 0.1 nm. The overall concentration of Pt or Pd in Co_3O_4 was measured with inductive coupling plasma (ICP). The reported Pt/Co or Pd/Co atomic ratios are the values measured with ICP. Ex situ XPS studies of catalysts were performed on the ambient pressure X-ray photoelectron spectroscopy system in our group.

In Situ Characterization during Catalysis. In situ studies of surface chemistry of catalysts were performed on the lab-based AP-XPS system in our group. The function of this in-house AP-XPS was demonstrated in our recent work.[23−31] Catalyst samples were transferred to a fixed-bed flow reactor which has gas inlet and outlet for in situ studies with a flowing mode. Reactant environment of in situ studies of Pt_1/Co_3O_4 and Pd_1/Co_3O_4 catalysts is a mixture of 1 Torr NO and 1 Torr of H_2. Pt 4f, Pt 4d, Pd 3d, Co 2p, O 1s, and C 1s were collected while a catalyst was in a reactive environment at different temperatures. C 1s of the substrate of HOPG was always taken as a reference after data acquisition at each reaction condition. Gas composition during catalysis in the catalysis reactor was monitored and online analyzed by using the quadrupole mass spectrometer.[32]

In situ X-ray absorption spectroscopy measurements of catalysts during catalysis were performed at the National Synchrotron Light Source, Brookhaven National Laboratory. The Pd K-edge measurements were performed at the X18B beamline in fluorescence mode, using a Lytle detector, and the Pt L_3 edge measurements at the X19A beamline, also in fluorescence mode, using a 4-channel Vortex detector. The samples were made by pressing the powders into circular pellets using a hydraulic press and transferred onto a sample holder of a Nashner-Adler in situ cell.[33] The cell is capable of heating the sample under a controlled atmosphere. X-ray absorption coefficients in metal Pt and Pd foils were measured in reference mode for X−ray energy calibration. Up to five consecutive scans were collected at each stage of the reaction to improve the signal-to-noise ratio.

The data in the XANES region of the absorption coefficient were examined by applying the same procedure for pre-edge line fitting, postedge curve fitting, and edge-step normalization to all data. EXAFS data analysis was performed with IFEFFIT package and FEFF6 theory. Data modeling at different temperatures was performed using standard procedures.[34,35] Several parameters describing electronic properties, specifically, the correction to the photoelectron energy origin, and local structural environment [coordination number (N), bond length (R)] and mean squared disorder parameter (σ^2) of the nearest neighbors around absorbing atoms were varied in the fit. More details of fitting were described in the section of Results and Discussion.

3. RESULTS AND DISCUSSION

3.1. Catalyst Consisting of Singly Dispersed Pt_1Co_m.

3.1.1. Single Dispersion of Pt Atoms on Co_3O_4 for 0.1% Pt/Co_3O_4. Figure 2 presents TEM images of pure Co_3O_4 nanorods we synthesized. The preferentially exposed surfaces are (1−10) and (001). They have an average size of ∼6 nm × ∼6 nm × ∼50−200 nm. Upon anchoring Pt atoms on Co_3O_4 nanorods, the morphology of nanorods basically remains, although some nanorods are broken into shorter ones. The measured interplanar distance of (220) of 0.1 atom % Pt/Co_3O_4, 2.82

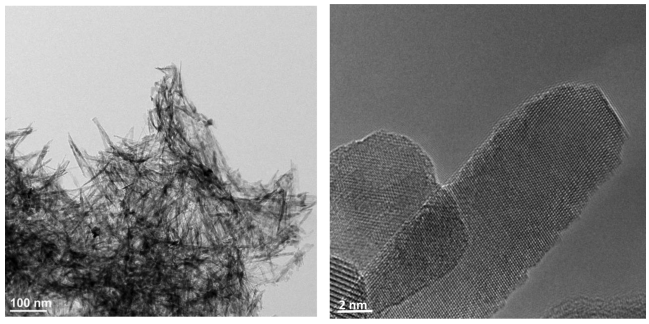

Figure 2. TEM images of Co_3O_4 nanorods. (a) Large-scale TEM image. (b) High-resolution TEM image.

DOI: 10.1021/acscatal.5b00842
ACS Catal. 2016, 6, 840−850

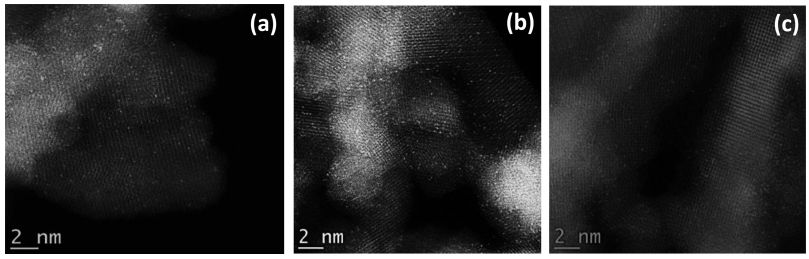

Figure 3. Images of aberration-corrected high-angle annular dark-field scanning transmission electron microscopy (HAADF-STEM) of 0.1 atom % Pt/Co_3O_4 with singly dispersed Pt atoms. Each bright spot is a Pt atom singly dispersed on Co_3O_4 nanorods.

Å is the same as pure Co_3O_4 nanorods. Thus, the impregnation of Pt atoms on Co_3O_4 does not change the lattice of Co_3O_4 because the immobilization of noble metal atoms on well-crystallized Co_3O_4 nanorods was done under a mild condition.

To identify the dispersion of Pt atoms on Co_3O_4 nanorods, the as-synthesized catalyst was examined with aberration-corrected high-angle annular dark-field scanning transmission electron microscopy (HAADF-STEM). Figure 3 presents the representative HAADF-STEM images of 0.1 atom % Pt/Co_3O_4 catalyst. Bright spots in images of Figure 3 are Pt atoms anchored on Co_3O_4. Under an assumption that all loaded Pt atoms are anchored on Co_3O_4 surface, coverage of Pt atoms on Co_3O_4 surface can be defined to the atomic ratio of all Pt atoms on the surface of Co_3O_4 to all Co atoms of the topmost layer of Co_3O_4 nanorods. With this definition, the theoretical coverage of Pt atoms is about 1.2% (see the calculation in Section 2 of the Supporting Information). Experimentally, the coverage of Pt atoms was measured through statistical accounting of bright spots (Pt atoms) in STEM images. This accounting gives the coverage of 1.5%, close to the theoretical atomic ratio of the anchored Pt atoms on surface to Co atoms of the surface, 1.2%. The difference between the ideal coverage of Pt atoms and the measured one could result from heterogeneous distribution of Pt atoms on surface of Co_3O_4 nanorods.

3.1.2. Single Dispersion of Pt Atoms on Co_3O_4 for 0.5 Atom % Pt/Co_3O_4. With the same synthetic route as the synthesis of 0.1 atom % Pt on Co_3O_4, 0.5 atom % Pt/Co_3O_4 was synthesized. Figure 4 presents the HAADF-STEM images of 0.5 atom % Pt/Co_3O_4. Compared to 0.1 atom % Pt- Co_3O_4 (Figure 3), Pt atoms of 0.5 atom % $Pt–Co_3O_4$ exhibit two types of dispersions. One is the single dispersion of Pt atoms; the second is a dispersion of Pt atoms, which are separated with a distance of 0.5–1.5 nm. The second type of dispersion was marked with red circles in Figure 4. Statistical accounting showed these fractions of singly dispersed Pt atoms in type I and II are ~52% and ~48%, respectively. Figure 5b is an enlargement of the second type of dispersion marked in Figure 5a. A close examination of the second type of dispersion found that Pt atoms in the second dispersion are not arranged into a lattice of a Pt nanocrystal. In fact, the distribution of these Pt atoms in Figure 5b is quite random. To make a better understanding of the random packing of Pt atoms in the second type of dispersion, Pt nanocrystals with a size of 2 nm supported on Co_3O_4 nanorods (Figure 5c–e) were examined with HAADF-STEM using the same data acquisition condition as Figure 5a,b. The crystallization of Pt nanoparticles in Figure 5c–e was confirmed with the measured lattice fringe. Because there is not any component of metallic Pt in spectra of Pt 4f and Pt 4d (to be discussed in Section 3.1.4) and no crystallographic lattice identified in the second type of dispersion (Figure 5a,b), it is inappropriate to assign the second type of dispersion (marked in red circles in Figure 4) to metallic nanoparticles of Pt. They are considered as

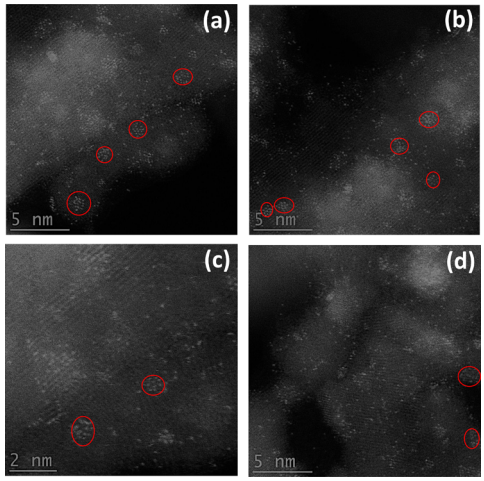

Figure 4. Images of aberration-corrected annular dark-field scanning transmission electron microscopy ((HAADF-STEM) of 0.5 atom % Pt/Co_3O_4 anchoring Pt atoms. Each bright spot with high contrast is a Pt atom on a Co_3O_4 nanorod. Red circles highlight the second type of dispersion of Pt atoms. (a), (b), (c), and (d) are representative images collected on a catalyst loaded on a TEM grid.

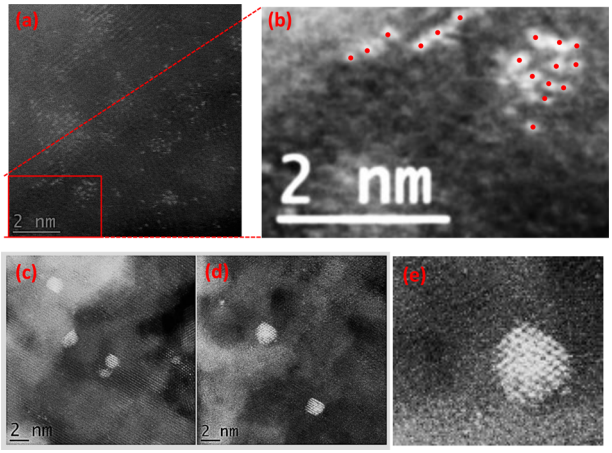

Figure 5. Images of aberration-corrected high-angle annular dark-field scanning transmission electron microscopy studies of catalyst of 0.5 atom % Pt/Co_3O_4 anchoring Pt atoms (a and b) and another catalyst, Pt nanoparticles impregnated on Co_3O_4 nanorods (c–e). In (a) and (b), each bright spot with a high contrast is a Pt atom annealed on Co_3O_4 nanorods. Bright spots are randomly dispersed. In (c), (d), and (e), Pt nanocrystals are clearly identified, and bright spots (Pt atoms) in nanoparticles are packed periodically.

DOI: 10.1021/acscatal.5b00842
ACS Catal. 2016, 6, 840–850

neighboring Pt atoms, which are anchored on Co_3O_4 surface at a relatively short distance.

Based on the method of calculations in Section 2 of the Supporting Information, loading of 0.5 atom % Pt to the surface of Co_3O_4 gives a surface coverage of 6.0%, which means there are 6 Pt atoms among every 100 Co atoms of the topmost layer of the Co_3O_4. As shown in Figures 4 and 5, these anchored Pt atoms on 0.5 atom % Pt/Co_3O_4 did not aggregate though some of them resided closely. The average distance between two adjacent Pt atoms in the first type of dispersion of 0.5 atom % Pt/Co_3O_4, ~3.5 nm, is definitely larger than the distance of 0.5−1.5 nm in the second type of dispersion. The reasons that these closely packed Pt atoms did not form a crystallographic lattice of Pt nanoparticles could be the relatively low surface coverage (6.0%). The annealing at an intermediate temperature in preparation could result in the close packing (Figure 5a) but not the formation of nanocrystal.

3.1.3. Formation of Catalyst Consisting of Singly Dispersed Pt_1Co_m. In situ XANES and EXAFS studies of Pt L_3 edge for Pt atoms of 0.5% Pt/Co_3O_4 were performed to explore the evolution of chemical states and coordination environment of the singly dispersed Pt atoms of this catalyst. Upon reduction at 300 °C, a very similar Pt L_3-edge feature collected at 25, 90, 150, 190, 250, and 300 °C during catalysis in the mixture of NO and H_2 was presented in Figure 6. The in situ XANES suggests a cationic state of Pt atoms during catalysis at these temperatures.

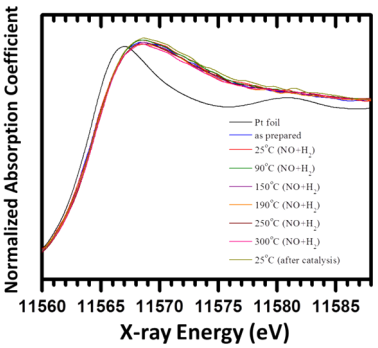

Figure 6. Pt L_3-edge XANES of 0.5 atom % Pt/Co_3O_4 catalysts during catalysis in the mixture of reactant gases (NO + H_2) in the temperature regime of 25−300 °C after reduction in 5% H_2 for a half hour.

In the analysis of data of the k^2-weighted Pt L_3-edge EXAFS spectra of 0.5 atom % Pt/Co_3O_4 as-synthesized and during catalysis (Figure 7), several models were carefully tried in fitting the experimental data. These models included Pt−Co, Pt−Pt, or Pt−O contributions, and any two or three of their combinations. Among all these trials of fittings, only a pure Pt−Co model gave adequate fits to the experimental data at these temperatures (Figure 7). Data were analyzed in the k-range from 2 to 10 $Å^{-1}$ and in the r-range from 1.7 Å to 2.8 Å. In order to reduce the number of variables, the spectra were analyzed concurrently, using the multiple data set fitting method, where multiple constraints were imposed on fitting variables to decrease correlation between them. The coordination number of Pt−Co pairs were constrained to be the same at all temperatures. The energy origin correction was constrained to be the same for all temperatures. The data and fits in r-space are shown in Figure 7. The best fitting result for the Pt−Co coordination number was 3.8 ± 0.3. The energy origin shift was −1.9 ± 0.7 eV. The best fitting results of Pt−Co distance and disordering parameters are given in Table 1. Thus, in situ EXAFS studies show that Pt atoms are singly anchored on the surface and a Pt atom chemically bonds to Co atoms upon H_2 reduction at 300 °C and during catalysis in the temperature range of 25−300 °C. Thus, the in situ EXAFS studies clearly suggest the formation of singly dispersed bimetallic sites, Pt_1Co_m.

3.1.4. Cationic State of Pt_1Co_m Sites during Catalysis. Catalysts 0.1 atom % Pt/Co_3O_4 and 0.5 atom % Pt/Co_3O_4 were reduced at 300 °C in 5% H_2. On the basis of the downshift of Pt 4d after the reduction, we would consider that there are oxygen atoms between Pt and Co before the removal of oxygen atoms by annealing at 300 °C in H_2. The removal of oxygen atoms by reduction in H_2 is supported by the formation of Pt−Co bonds identified with EXAFS (Figure 7 and Table 1). The reduction process can remove oxygen atoms between Pt and Co because Pt atoms can catalyze the dissociation of molecular hydrogen to atomic hydrogen; the formed atomic hydrogen can spillover from Pt atom to the oxygen atom between Pt and Co to form a OH group, and the OH group can bond with another hydrogen atom to form a H_2O molecule and then desorb from the surface. Upon removal of the oxygen atoms between Pt and Co, the Pt atom directly bonds with one or more Co atoms. The formation of Pt−Co bonds was confirmed by the EXAFS studies.

In situ studies of surface chemistry of 0.1 atom % Pt/Co_3O_4 and 0.5 atom % Pt/Co_3O_4 under reaction condition of a mixture of NO and H_2 were performed on our lab-based AP-XPS system[32,36] in order to identify whether Pt_1Co_m is at a metallic state or a cationic state during catalysis. Figure 8 presents photoemission features of Co 2p and Pt 4d of 0.1 atom % Pt/Co_3O_4 and 0.5% Pt/Co_3O_4. Two main peaks of Co 2p are clearly observed at 780.5 and 796.0 eV, which are consistent with the peak positions of Co $2p_{3/2}$ and Co $2p_{1/2}$ of Co_3O_4 reported in literature.[37−42] Notably, such photoemission feature of Co 2p is preserved in the entire temperature regime of 25−300 °C during catalysis (Figure 8a,c). The lack of the characteristic photoemission feature of Co^{2+} of CoO, a pair of satellite peaks at ~786.4 eV and ~803.0 eV attributed to the Co^{2+} ions at an octahedral site, shows the preservation of Co_3O_4 surface phase during catalysis. The preservation of the photoemission feature of Co_3O_4 surface in the mixture of both NO and H_2 could result from the coexistence of both a strong oxidative gas, NO and a reductive gas, H_2 during catalysis.

Figure 8b,d are Pt 4d photoemission features of 0.1 atom % Pt/Co_3O_4 and 0.5 atom % Pt/Co_3O_4, respectively. The binding energy at 317.0 eV in Pt 4d spectra clearly excludes the possibility of a metallic state in terms of formation of Pt nanoparticles in the temperature regime of 25−300 °C because the Pt $4d_{5/2}$ peak of metallic Pt is only 315.0 eV.[43] In fact, the binding energy of Pt 4d at 317.0 eV is consistent with Pt 4d of Pt cations of platinum oxide reported in the literature.[44,45] Obviously, the evolutions of Pt 4d (Figure 8) and Pt 4f (Figure S6) in AP-XPS studies indicate the lack of metallic Pt nanoparticles during catalysis. These singly dispersed Pt atoms did not aggregate into metallic Pt nanoparticles on the Co_3O_4 surface during catalysis at a temperature ≤300 °C; these Pt atoms are still in a cationic state. A comparative in situ study of 0.5 atom % Pt/SiO_2 during catalysis using AP-XPS (Figure S7 in Supporting Information) was performed under the same reaction conditions as 0.5 atom % Pt/Co_3O_4. As shown in Figure S7, platinum in the as-synthesized 0.5 atom % Pt/SiO_2

DOI: 10.1021/acscatal.5b00842
ACS Catal. 2016, 6, 840−850

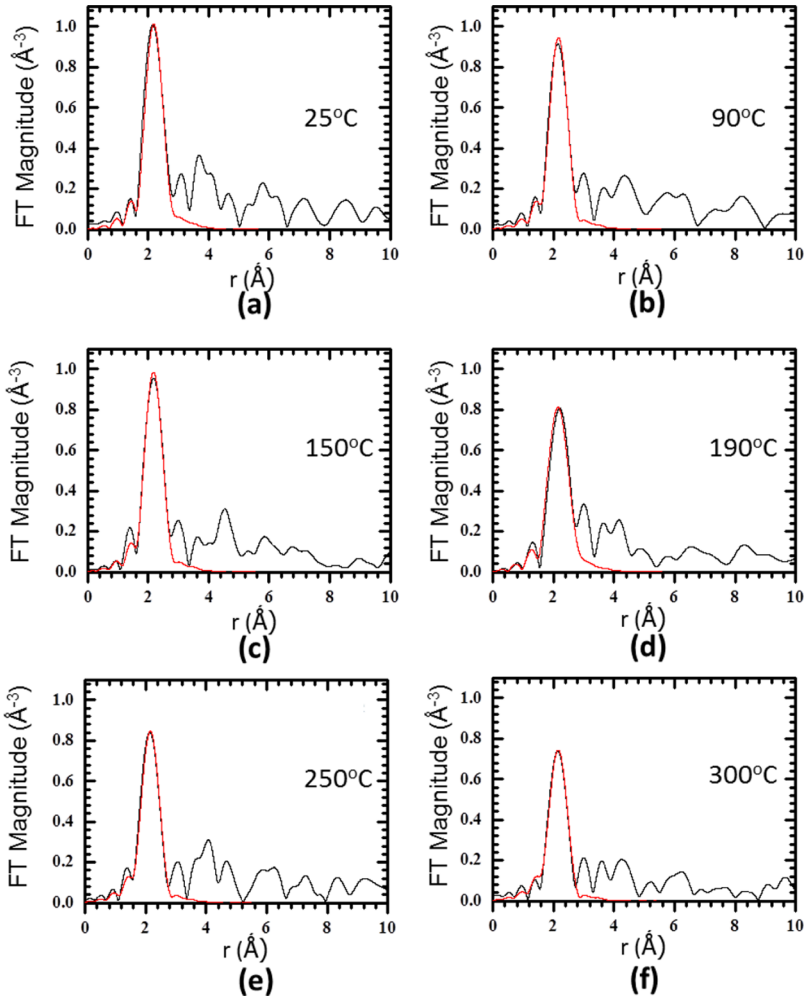

Figure 7. In situ EXAFS data and theoretical fits of 0.5 atom % Pt/Co_3O_4 during catalysis in the temperature regime of 25−300 °C after reduction at 300 °C in 5% H_2 for a half hour. Experimental and fitted data are shown in black and red, respectively.

Table 1. Fitting Results Obtained by EXAFS Analysis for Pt−Co Coordination Numbers, Distances, and Disorder Parameters of 0.5 Atom % Pt/Co_3O_4 during Catalysis after Annealing in 5% H_2

T (°C)	CN (Pt−Co)	CN (Pt−O)	R (Pt−Co) (Å)	σ^2 (Å^2)
25 °C	3.8 ± 0.3	0	2.61 ± 0.01	0.0056 ± 0.0008
90 °C	3.8 ± 0.3	0	2.60 ± 0.01	0.0078 ± 0.0008
150 °C	3.8 ± 0.3	0	2.60 ± 0.01	0.0074 ± 0.0007
190 °C	3.8 ± 0.3	0	2.61 ± 0.01	0.0081 ± 0.0008
250 °C	3.8 ± 0.3	0	2.60 ± 0.01	0.0090 ± 0.0008
300 °C	3.8 ± 0.3	0	2.60 ± 0.01	0.0102 ± 0.0010

exists in an oxidizing state at room temperature. However, it is reduced to a metallic state at 250 °C in the mixture of NO and H_2 (1:1). Obviously, the active phase of 0.5 atom % Pt/SiO_2 in NO reduction with H_2 is Pt atoms at a metallic state (Figure S7). In contrast to 0.5 atom % Pt/SiO_2, the preservation of oxidizing state of Pt atoms of 0.1 atom % Pt/Co_3O_4 and 0.5 atom % Pt/Co_3O_4 up to 300 °C during catalysis (Figures 8b,d and S6) clearly shows that the coordination environments of Pt atoms of 0.1 atom % Pt/Co_3O_4 and 0.5 atom % Pt/Co_3O_4 are distinctly different from that of 0.5 atom % Pt/SiO_2. These in situ studies of AP-XPS clearly show that Pt atoms of singly dispersed bimetallic sites are in a cationic state.

3.1.5. Catalytic Performance of Catalyst Consisting of Singly Dispersed Bimetallic Sites Pt_1Co_m. The above in situ EXAFS and in situ AP-XPS studies have confirmed the formation of singly dispersed bimetallic sites Pt_1Co_m and this electronic state and structure remain during catalysis. The following catalysis studies clearly show it is highly active for reduction of NO with H_2. Figure 9 presents catalytic performance in reduction of nitric oxide with H_2 ($2NO + 2H_2 = N_2 + 2H_2O$) on 0.5 atom % Pt/Co_3O_4.

The catalyst 0.5 atom % Pt/Co_3O_4 exhibits a high selectivity to production of N_2 (Figure 9). In fact, selectivity for production of N_2 of 0.5 atom % Pt/Co_3O_4 is already 98% at 150 °C. The high selectivity of 0.5 atom % Pt/Co_3O_4 at 150 °C could be related to its high conversion of NO. Because the conversion of 0.5 atom % Pt/Co_3O_4 is almost 100% at a temperature ≥150 °C, there is no remaining nitric oxide around this catalyst. Thus, N_2O cannot be formed because N_2O is typically formed through a coupling of an NO molecule with a nitrogen atom dissociated from NO. As shown in Figure S9b, parallel studies of Pt metallic nanoparticles supported on SiO_2 (200 mg of 0.5 atom % Pt/SiO_2), 250 mg of pure Co_3O_4 support and 100 mg of 0.5 atom % Pt/Co_3O_4 under the same condition of catalytic measurement showed they exhibit the same conversion of NO, 100% at 250 °C; however, 0.5 atom % Pt/Co_3O_4 exhibits a much higher catalytic selectivity for

DOI: 10.1021/acscatal.5b00842
ACS Catal. 2016, 6, 840−850

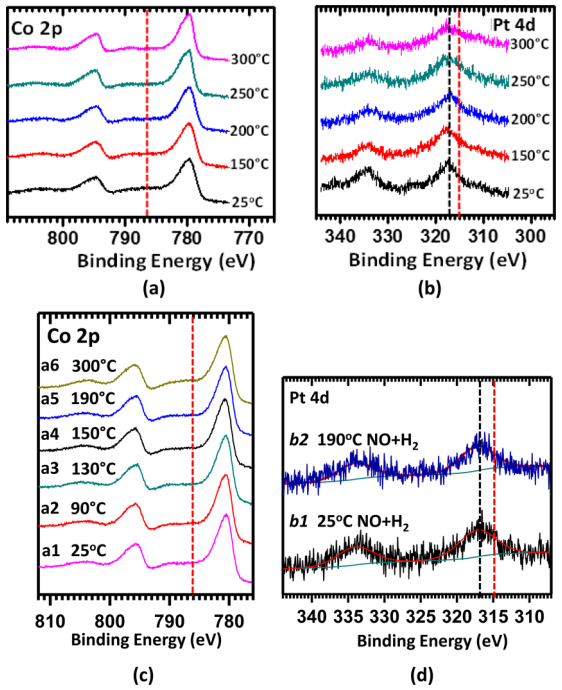

Figure 8. Photoemission features of Co 2p and Pt 4d of the as-synthesized 0.1 atom % Pt/Co_3O_4 and 0.5 atom % Pt/Co_3O_4 after reduction at 300 °C in 5% H_2 for half an hour in a flow reactor integrated to AP-XPS. The pressure in the reactor during data acquisition is 1 Torr NO and 1 Torr H_2. (a) Co 2p of 0.1 atom % Pt/Co_3O_4; (b) Pt 4d of 0.1 atom % Pt/Co_3O_4; (c) Co 2p of 0.5 atom % Pt/Co_3O_4; (d) Pt 4d of 0.5 atom % Pt/Co_3O_4. The red lines on (a) and (c) mark the position of satellite peak of Co $2p_{3/2}$ of Co^{2+} of CoO. The red lines in (b) and (d) mark the position of metallic Pt $4d_{5/2}$.

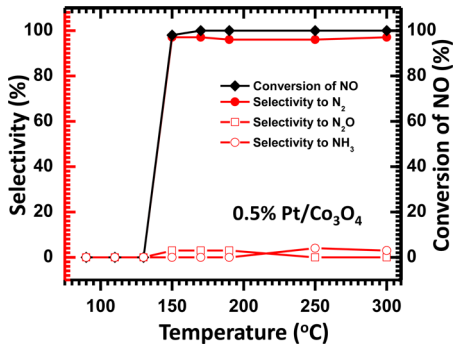

Figure 9. Catalytic performances of 100 mg of 0.5 atom % Pt/Co_3O_4. Conversion is shown in black lines and black axes. Selectivity is shown in red lines and red axes. Selectivities to N_2, N_2O, and NH_3 are shown in solid circle, hollow cube, and hollow circle, respectively.

production of N_2 at this temperature than 0.5 atom % Pt/SiO_2 and pure Co_3O_4 (Figure S9a). In addition, as shown in Figure 10, 100 mg of 0.5 atom % Pt/SiO_2 is not active at 170 °C while 100 mg of 0.5 atom % Pt/Co_3O_4 exhibits conversion of ~98% at this temperature. Clearly, 0.5 atom % Pt/Co_3O_4 exhibits a much better catalytic performance than 0.5 atom % Pt/SiO_2 and pure Co_3O_4. This difference in catalytic selectivity suggests that the formed Pt_1Co_m sites are definitely different from that of catalytic sites of Pt nanoparticles supported on SiO_2 in the case of 0.5 atom % Pt/SiO_2. More importantly, Pt nanoparticles supported on Co_3O_4 in the case of 100 mg of 5 atom % Pt/Co_3O_4 exhibit a lower selectivity for the production of N_2 compared to 100 mg of 0.5 atom % Pt/Co_3O_4 in the temperature range of 150−300 °C, although 100 mg of 0.5 atom % Pt/Co_3O_4 and 100 mg of 5 atom % Pt/Co_3O_4 exhibit the same conversion of NO in the temperature range of 150−300 °C (Figure 10). The difference in catalytic selectivity between 0.5 atom % Pt/Co_3O_4 and 5 atom % Pt/Co_3O_4 while they exhibit the same conversion suggests that the singly dispersed bimetallic sites Pt_1Co_m supported on Co_3O_4 in the case of 0.5 atom % Pt/Co_3O_4 are distinctly different from the catalytic sites of surface of Pt nanoparticles supported on Co_3O_4.

Overall, these in situ studies of AP-XPS, XANES, and EXAFS allow for building a correlation of surface chemistry of these catalysts consisting of singly dispersed bimetallic sites during catalysis and their corresponding catalytic performances. This correlation suggests that the singly dispersed bimetallic sites Pt_1Co_m are active sites for the reduction of NO with H_2.

3.2. Catalyst Consisting of Singly Dispersed Pd_1Co_n.

3.2.1. Formation of Catalyst Consisting of Singly Dispersed Pd_1Co_n. The catalyst 0.5 atom % Pd/Co_3O_4 was prepared with the exactly same method as 0.5 atom % Pt/Co_3O_4. However, HAADF-STEM does not readily distinguish Pd from Co atoms. The difference in contrast of two atoms in HAADF-STEM imaging technique relies on the detection of electrons scattered at high angles relative to the transmitted beam using an annular detector. At large scattering angles the number of electrons detected is strongly and quantitatively dependent on the atomic number (Z) of the atoms interacting with the electron beam. The signal, directly related to the contrast in images is proportional to Z^x and other factors.[46] As Pd and Co are 4d and 3d blocks, respectively, the contrast between Pd and Co is much smaller than that between Pt and Co. Thus, it is quite challenging to distinguish Pd from Co with HAADF-STEM readily. Fortunately, EXAFS and AP-XPS helped the identification of binding environment and oxidation state of Pd of 0.5 atom % Pd/Co_3O_4, respectively. Particularly, in situ EXAFS studies measured the coordination number of neighboring atoms to a Pd atom of 0.5 atom % Pd/Co_3O_4 during catalysis. Figure 11 presents k-space data of the k^2-weighted Pd K-edge EXAFS spectra of 0.5 atom % Pd/Co_3O_4 as-synthesized and during catalysis. EXAFS of metallic Pd foil at 25 °C (black line) was included for a comparison. The data in Figure 12a can be visually divided into two groups: the 25 °C (pink), 100 °C (orange), and 150 °C (gray) (the first group, corresponding to the first half of the reaction cycle) and the 200 °C (red), 300 °C (green), and 25 °C (blue) (the second group, corresponding to the second half of the reaction cycle). There is an obvious change between the two groups, while the data within each group appear very similar.

Analysis and theoretical fitting of the data of EXAFS (Figure 12 and Table 2) show that (1) a Pd atom bonds with two or three oxygen atoms with a bond length of 2.00 ± 0.02 Å in the temperature range of 25−150 °C in the mixture of NO and H_2 and (2) the coordination number of O to Pd is 2.7 ± 0.6 at 25 °C, 100 °C, and 150 °C (Table 2). More importantly, the lack of coordination of Pd to Pd atoms and Pd to Co in 0.5% Pd/Co_3O_4 at a temperature regime ≤150 °C shows that (1) Pd atoms are anchored on oxygen atoms of Co_3O_4 and (2) Pd atoms are singly dispersed.

A change of the chemical state of Pd atoms between 150 and 200 °C was suggested by AP-XPS study (Figure 13b) and XANES (Figure S8) as well. EXAFS analysis attributed the down-shift of Pd 3d binding energy to the significant changes in coordination environment of Pd atoms during catalysis when

DOI: 10.1021/acscatal.5b00842
ACS Catal. 2016, 6, 840−850

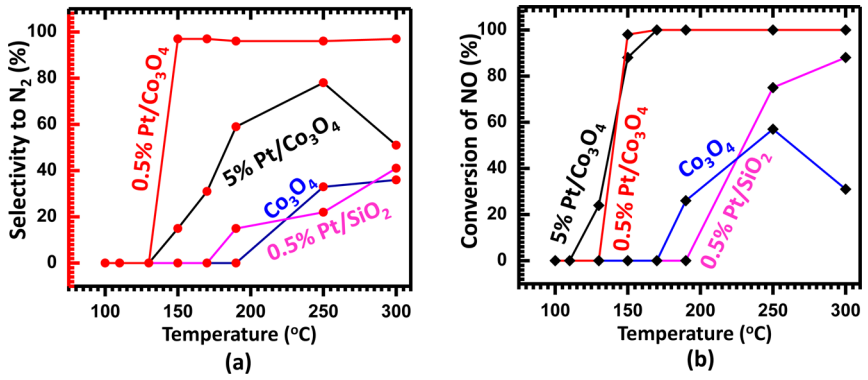

Figure 10. Comparison of catalytic selectivities (a) and activities (b) of 100 mg of 0.5 atom % Pt/Co_3O_4, 100 mg of 5 atom % Pt/Co_3O_4, 100 mg of pure Co_3O_4, and 100 mg of 0.5 atom % Pt/SiO_2 under the same catalytic conditions.

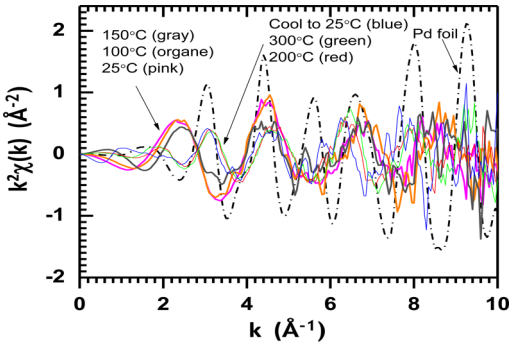

Figure 11. k-space of the k^2-weighted Pd K-edge EXAFS spectra of 0.5% Pd/Co_3O_4 during catalysis in the temperature regime of 25−300 °C.

the catalyst was annealed from 150 to 200 °C (Table 2). The bond lengths of Pd−O and Pd−Co and coordination environment of Pd atoms listed in Table 2 clearly suggest a change of bonding environment of singly dispersed Pd at this temperature regime (150−200 °C). Obviously, bonding atoms of a Pd atom are switched from oxygen to cobalt at a temperature between 150 and 200 °C. This restructuring forms Pd_1Co_n nanoclusters. Here Pd_1Co_n is a symbolic notation, and the clusters may range from Pd_1Co_4 to Pd_1Co_6 based on our measurement and analysis (Table 2), with the average coordination number, *n*.

3.2.2. Cationic State of Pd_1Co_n Sites. Surface chemistry of 0.5 atom % Pd/Co_3O_4 was studied during catalysis by using AP-XPS (Figure 13). Two peaks of Co 2p were observed at 780.5 and 796.0 eV, respectively, attributed to Co $2p_{3/2}$ and Co $2p_{1/2}$ (Figure 13a). These photoemission features are consistent with those of Co_3O_4 reported in literature.[37−42] The lack of photoemission feature at 786.4 and 803.0 eV of CoO clearly shows that Co_3O_4 is maintained during catalysis up to 250 °C.

In terms of Pd 3d, the binding energy at 100 °C is 337.6 eV (Figure 13b), similar to Pd 3d of PdO_x.[43,47−49] It is noted that Pd 3d down-shifts by 0.8 to 336.8 eV at 200 °C in contrast to those at 100 °C. The peak position of Pd 3d at 200 °C remains the same up to 300 °C. Obviously, Pd is not reduced to metallic Pd during catalysis even at a temperature of 250 °C (Figure 13b3).

3.2.3. Catalytic Performance of Catalyst Consisting of Singly Dispersed Bimetallic Sites Pd_1Co_n. Figure 14 presents catalytic performances of both 0.5 atom % Pd/Co_3O_4 and 0.5 atom % Pd/SiO_2. There is no conversion of nitric oxide at a temperature of 100 °C. At 150 °C, selectivity to production of N_2 on 0.5 atom % Pd/Co_3O_4 is ∼70% and reaches 98% at 250 °C (Figure 14a). As catalytic selectivity for production of N_2 through reduction of NO with H_2 depends on catalytic activity, we prefer to compare the catalytic selectivity for production of N_2 on 0.5 atom % Pd/Co_3O_4 to 0.5 atom % Pd/SiO_2 at the same conversion measured under the exactly same catalytic condition. As shown in Figure 14, catalytic selectivity for production of N_2 at 250 °C is 97% on 0.5 atom % Pd/Co_3O_4 and 39% on 0.5 atom % Pd/SiO_2 though the conversions of

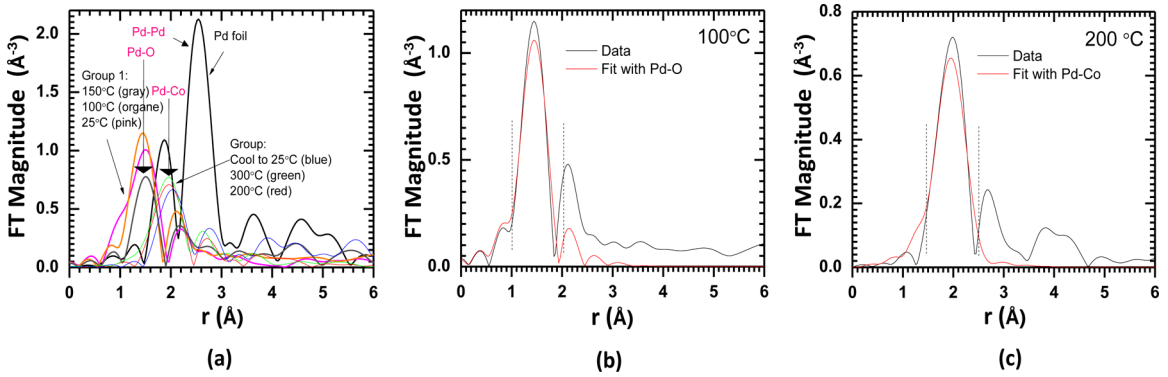

Figure 12. Data analysis and theoretical fits of 0.5 atom % Pd/Co_3O_4 during catalysis in the temperature regime of 25−300 °C. For comparison, data of metallic Pd foil was included as well. (a) Experiments data collected. (b) and (c): Examples of fitting with Pd−O of 0.5 atom % Pd/Co_3O_4 at 100 °C and Pd−Co of 0.5 atom % Pd/Co_3O_4 at 200 °C, respectively.

DOI: 10.1021/acscatal.5b00842
ACS Catal. 2016, 6, 840−850

Table 2. Coordination Numbers, Bond Lengths, and Their Disordering of Pd Atoms and Its Nearest Neighboring Atoms of 0.5 Atom % Pd/Co_3O_4 during Catalysis at 25−300 °C in the Mixture of NO and H_2 Studied with EXAFS

temperature of catalysis (°C)	N (Pd−O)	R (Pd−O) (Å)	σ^2 (Pd−O) (Å^2)	N (Pd−Co)	R (Pd−Co) (Å)	σ^2 (Pd−Co) (Å^2)
25	2.7 ± 0.6	2.00 ± 0.02	0.001 ± 0.004			
100	2.7 ± 0.6 (fit)	1.99 ± 0.02	0.000 ± 0.003			
150	2.7 ± 0.6 (fit)	2.02 ± 0.03	0.006 ± 0.005			
250				5.0 ± 1.3	2.53 ± 0.02	0.013 ± 0.003
300				5.0 ± 1.3 (fit)	2.51 ± 0.02	0.012 ± 0.003
25 (cool from 300 °C)				5.0 ± 1.3 (fit)	2.58 ± 0.02	0.013 ± 0.004

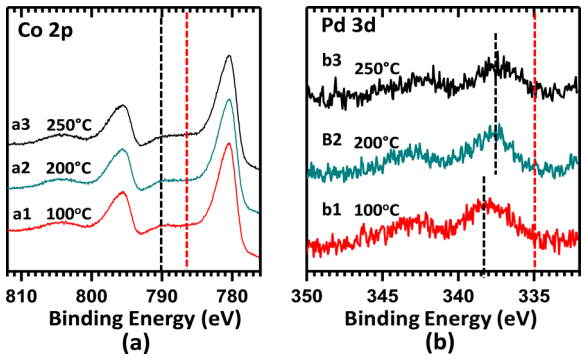

Figure 13. In situ AP-XPS studies of (a) Co 2p and (b) Pd 3d of the as-synthesized 0.5 atom % Pd/Co_3O_4 in a flow reactor integrated to AP-XPS. The reactant gas is a mixture of 1 Torr NO and 1 Torr H_2. In (a), the red dash line marked the position of the satellite peak of Co $2p_{3/2}$ of CoO if any. The black dash line marks the weak satellite peak of Co $2p_{3/2}$ of Co^{3+} of Co_3O_4. In (b), the red dash line marks the peak position of Pd $3d_{5/2}$ of metallic Pd.

NO on both 0.5 atom % Pd/Co_3O_4 and 0.5 atom % Pd/SiO_2 at 250 °C are 100%.

3.2.4. Correlation between Geometric Structure and Electronic State of Pd_1Co_n Site. The change of coordination environment of Pd atoms in the temperature regime of 150−200 °C (Table 2) is consistent with the temperature range of 150−200 °C (Figure 14a) where the catalysis turns on. The correlation *between* the change of bonding environment of Pd atoms of 0.5 atom % Pd/Co_3O_4 during catalysis at 150−250 °C *and* the large increase of catalytic selectivity in this temperature range suggests that Pd_1Co_n/Co_3O_4 formed through restructuring in the temperature range of ≤250 °C is responsible for the high selectivity (98%) for production of N_2 in the reduction of NO with H_2 (Figure 14a). In addition, the catalytic selectivity to N_2 on 0.5 atom % Pd/Co_3O_4 in the second-run catalysis measurement after it was cooled to room temperature from the reaction condition (300 °C in the gas mixture of NO and H_2) increases in the temperature range of 125−225 °C (Supporting Information Figure S10) compared to that in the first run. The increase of N_2 selectivity is attributed to the formation of singly dispersed Pd_1Co_n bimetallic sites in the temperature range of 125−225 °C in the first run. Thus, the active sites responsible for high selectivity at 250 °C are singly dispersed Pd_1Co_n. The in situ EXAFS studies during catalysis at 250 °C show that Pd_1Co_n nanoclusters remain their single dispersion up to 300 °C during catalysis (Table 2).

The loss of surface lattice oxygen atoms of Co_3O_4 by reducing the catalyst precursor of 0.5 atom % Pd/Co_3O_4 makes a Pd atom bond with five neighboring cobalt atoms (Table 2). The high activity of surface lattice oxygen atoms of pure Co_3O_4 was suggested as the driving force of the high activity of CO oxidation of Co_3O_4 at a low temperature;[22] the low energy barrier of 0.26 eV for hopping of oxygen vacancies of Co_3O_4 was reported in the literature.[14] Upon surface lattice oxygen atoms are removed by an external species such as hydrogen atoms, the Co atoms originally bonded to an absorbed oxygen atom, are under-coordinated. Then, the Pd atom can readily bond with the under-coordinated cobalt atoms to form a cluster through surface thermal diffusion of Pd atoms. Removal of a portion of oxygen atoms does not result in the aggregation of Pd atoms since there is lack of Pd−Pd bonds. Upon removal of an oxygen atom originally bonded between a Pd atom and a Co atom, the Pd atom can immediately bond to its surrounding Co atoms. The immediate bonding with Co atoms is thermodynamically and kinetically favorable for Pd atoms in contrast to a potential aggregation of two Pd atoms as the average distance between two singly dispersed Pd atoms is 2−3 nm in the case of 0.1 atom % Pd/Co_3O_4. This distance is much larger than the

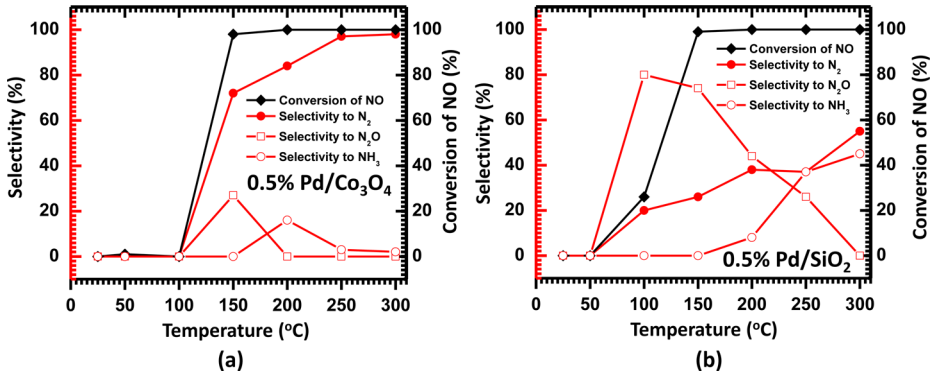

Figure 14. Catalytic performances of (a) 100 mg of 0.5 atom % Pd/Co_3O_4 and (b) 100 mg of 0.5 atom % Pd/SiO_2. Conversion is shown in black lines and black axes. Selectivity is shown in red lines and red axes. Selectivities to N_2, N_2O, and NH_3 are shown in solid circle, hollow cube, and hollow circle, respectively.

DOI: 10.1021/acscatal.5b00842
ACS Catal. 2016, 6, 840−850

distance between a Pd atom and its interval Co atoms (Pd−O−Co), 2−3 Å. In fact, the coverage of Pd atoms on surface of a Co_3O_4 nanorod is only 6% even for 0.5 atom % Pd/Co_3O_4 under an assumption that all Pd atoms are dispersed on surfaces of Co_3O_4 nanorods. The coverage of 6% can be calculated using the method in Section 2 of Supporting Information.

The successful development of the single site bimetallic catalyst Pd_1Co_n suggests that the formation of singly dispersed bimetallic sites on a reducible oxide is a method to develop a catalyst by anchoring singly dispersed metal atoms on a reducible oxide with a following calcination in H_2. These in situ characterizations of chemical state and coordination environment of singly dispersed bimetallic sites during catalysis and measurements of catalytic performances well demonstrated this new method.

4. SUMMARY

Catalysts consisting of singly dispersed bimetallic sites Pt_1Co_m or Pt_1Co_n anchored on Co_3O_4 are active for reduction of NO with H_2 with 98% selectivity for production of N_2 at 150 °C. In contrast to the outstanding catalytic performance of Pt_1Co_m, Pt nanoparticles supported on SiO_2 are not active for the reaction at 150 °C. In situ studies suggested that sites responsible for the 98% selectivity in reducing NO with H_2 are the singly dispersed bimetallic site Pt_1Co_m. Pt_1Co_m sites anchored on Co_3O_4 in 0.5 atom % Pt/Co_3O_4 are singly distributed in the temperature regime of 25−300 °C during catalysis. Singly dispersed bimetallic sites Pd_1Co_n of 0.5 atom % Pd/Co_3O_4 are responsible for selective reduction of nitric oxide with hydrogen. Pd_1Co_n sites supported on Co_3O_4 are still singly dispersed up to 300 °C during catalysis. The successful development of catalysts consisting of singly dispersed bimetallic sites Pt_1Co_m or Pd_1Co_n highly selective in reduction of nitric oxide with hydrogen illustrates a route to develop new bimetallic catalysts with high selectivity and a new type of single site catalysts.

■ ASSOCIATED CONTENT

Supporting Information

The Supporting Information is available free of charge on the ACS Publications website at DOI: 10.1021/acscatal.5b00842.

Additional figures and schemes (PDF)

■ AUTHOR INFORMATION

Corresponding Authors

*E-mail: franklin.feng.tao@ku.edu.
*E-mail: frenkel@bnl.gov.

Author Contributions

‖L.N. and S.Z. contributed to this work equally.

Notes

The authors declare no competing financial interest.

■ ACKNOWLEDGMENTS

This work is supported by Chemical Catalysis program of U.S. National Science Foundation career award under grant NSF-CHE 1462121. A.I.F. acknowledges support from the U.S. Department of Energy Grant No. DE-FG02-03ER15476. Beamline X19A at the NSLS is supported in part by the Synchrotron Catalysis Consortium, U.S. Department of Energy Grant No. DE-FG02-05ER15688. The authors appreciate X. Zhang for help in some experiments of catalytic studies.

■ REFERENCES

(1) Chen, M. S.; Kumar, D.; Yi, C. W.; Goodman, D. W. *Science* **2005**, *310*, 291.
(2) Besenbacher, F.; Chorkendorff, I.; Clausen, B. S.; Hammer, B.; Molenbroek, A. M.; Norskov, J. K.; Stensgaard, I. *Science* **1998**, *279*, 1913.
(3) Kyriakou, G.; Boucher, M. B.; Jewell, A. D.; Lewis, E. A.; Lawton, T. J.; Baber, A. E.; Tierney, H. L.; Flytzani-Stephanopoulos, M.; Sykes, E. C. H. *Science* **2012**, *335*, 1209.
(4) Hammond, C.; Dimitratos, N.; Jenkins, R. L.; Lopez-Sanchez, J. A.; Kondrat, S. A.; ab Rahim, M. H.; Forde, M. M.; Thetford, A.; Taylor, S. H.; Hagen, H.; Stangland, E. E.; Kang, J. H.; Moulijn, J. M.; Willock, D. J.; Hutchings, G. J. *ACS Catal.* **2013**, *3*, 689.
(5) Hammond, C.; Forde, M. M.; Ab Rahim, M. H.; Thetford, A.; He, Q.; Jenkins, R. L.; Dimitratos, N.; Lopez-Sanchez, J. A.; Dummer, N. F.; Murphy, D. M.; Carley, A. F.; Taylor, S. H.; Willock, D. J.; Stangland, E. E.; Kang, J.; Hagen, H.; Kiely, C. J.; Hutchings, G. J. *Angew. Chem., Int. Ed.* **2012**, *51*, 5129.
(6) Groothaert, M. H.; Smeets, P. J.; Sels, B. F.; Jacobs, P. A.; Schoonheydt, R. A. *J. Am. Chem. Soc.* **2005**, *127*, 1394.
(7) Smeets, P. J.; Hadt, R. G.; Woertink, J. S.; Vanelderen, P.; Schoonheydt, R. A.; Sels, B. F.; Solomon, E. I. *J. Am. Chem. Soc.* **2010**, *132*, 14736.
(8) Shan, J.; Huang, W.; Nguyen, L.; Yu, Y.; Zhang, S.; Li, Y.; Frenkel, A. I.; Tao, F. *Langmuir* **2014**, *30*, 8558.
(9) Sun, S. H.; Zhang, G. X.; Gauquelin, N.; Chen, N.; Zhou, J. G.; Yang, S. L.; Chen, W. F.; Meng, X. B.; Geng, D. S.; Banis, M. N.; Li, R. Y.; Ye, S. Y.; Knights, S.; Botton, G. A.; Sham, T. K.; Sun, X. L. *Sci. Rep.* **2013**, *3*, 1775.
(10) Hashimoto, A.; Takeguchi, M. *J. Electron Microsc.* **2012**, *61*, 409.
(11) Qiao, B. T.; Wang, A. Q.; Yang, X. F.; Allard, L. F.; Jiang, Z.; Cui, Y. T.; Liu, J. Y.; Li, J.; Zhang, T. *Nat. Chem.* **2011**, *3*, 634.
(12) Hu, Z. P.; Metiu, H. *J. Phys. Chem. C* **2011**, *115*, 17898.
(13) Zhang, S.; Nguyen, L.; Liang, J.-X.; Shan, J.; Liu, J.; Frenkel, A. I.; Patlolla, A.; Huang, W.; Li, J.; Tao, F. *Nat. Comm.* **2015**, *6*, 7938.
(14) Jiang, D.-e.; Dai, S. *Phys. Chem. Chem. Phys.* **2011**, *13*, 978.
(15) Hamada, H.; Haneda, M. *Appl. Catal., A* **2012**, *421*, 1.
(16) Savva, P. G.; Costa, C. N. *Catal. Rev.: Sci. Eng.* **2011**, *53*, 91.
(17) Granger, P.; Dhainaut, F.; Pietrzik, S.; Malfoy, P.; Mamede, A. S.; Leclercq, L.; Leclercq, G. *Top. Catal.* **2006**, *39*, 65.
(18) Furfori, S.; Russo, N.; Fino, D.; Saracco, G.; Specchia, V. *Chem. Eng. Sci.* **2010**, *65*, 120.
(19) Costa, C. N.; Savva, P. G.; Andronikou, C.; Lambrou, P. S.; Polychronopoulou, K.; Belessi, V. C.; Stathopoulos, V. N.; Pomonis, P. J.; Efstathiou, A. M. *J. Catal.* **2002**, *209*, 456.
(20) Costa, C. N.; Stathopoulos, V. N.; Belessi, V. C.; Efstathiou, A. M. *J. Catal.* **2001**, *197*, 350.
(21) Machida, M.; Ikeda, S.; Kurogi, D.; Kijima, T. *Appl. Catal., B* **2001**, *35*, 107.
(22) Xie, X. W.; Li, Y.; Liu, Z. Q.; Haruta, M.; Shen, W. J. *Nature* **2009**, *458*, 746.
(23) Si, R.; Tao, J.; Evans, J.; Park, J. B.; Barrio, L.; Hanson, J. C.; Zhu, Y.; Hrbek, J.; Rodriguez, J. A. *J. Phys. Chem. C* **2012**, *116*, 23547.
(24) Wen, C.; Zhu, Y.; Ye, Y.; Zhang, S.; Cheng, F.; Liu, Y.; Wang, P.; Tao, F. *ACS Nano* **2012**, *6*, 9305.
(25) Zhu, Y.; Zhang, S.; Ye, Y.; Zhang, X.; Wang, L.; Zhu, W.; Cheng, F.; Tao, F. *ACS Catal.* **2012**, *2*, 2403.
(26) Shan, J.; Zhu, Y.; Zhang, S.; Zhu, T.; Rouvimov, S.; Tao, F. *J. Phys. Chem. C* **2013**, *117*, 8329.
(27) Nguyen, L.; Zhang, S.; Yoon, S. J.; Tao, F. *ChemCatChem* **2015**, *7*, 2346.
(28) Shan, J.-j.; Nguyen, L.; Zhang, S.; Tao, F.-F. *Catal. Lett.* **2015**, *145*, 1571.
(29) Tao, F. F.; Shan, J.-j.; Nguyen, L.; Wang, Z.; Zhang, S.; Zhang, L.; Wu, Z.; Huang, W.; Zeng, S.; Hu, P. *Nat. Commun.* **2015**, *6*, 7798.

DOI: 10.1021/acscatal.5b00842
ACS Catal. 2016, 6, 840−850

(30) Zhang, S.; Shan, J.-j.; Zhu, Y.; Frenkel, A. I.; Patlolla, A.; Huang, W.; Yoon, S. J.; Wang, L.; Yoshida, H.; Takeda, S.; Tao, F. *J. Am. Chem. Soc.* **2013**, *135*, 8283.
(31) Zeng, S.; Nguyen, L.; Cheng, F.; Liu, L.; Yu, Y.; Tao, F. *Appl. Surf. Sci.* **2014**, *320*, 225.
(32) Tao, F. *Chem. Commun.* **2012**, *48*, 3812.
(33) Nashner, M. S.; Frenkel, A. I.; Adler, D. L.; Shapley, J. R.; Nuzzo, R. G. *J. Am. Chem. Soc.* **1997**, *119*, 7760.
(34) Frenkel, A. I.; Hills, C. W.; Nuzzo, R. G. *J. Phys. Chem. B* **2001**, *105*, 12689.
(35) Sanchez, S. I.; Menard, L. D.; Bram, A.; Kang, J. H.; Small, M. W.; Nuzzo, R. G.; Frenkel, A. I. *J. Am. Chem. Soc.* **2009**, *131*, 7040.
(36) Tao, F. *ChemCatChem* **2012**, *4*, 583.
(37) Chuang, T. J.; Brundle, C. R.; Rice, D. W. *Surf. Sci.* **1976**, *59*, 413.
(38) Langell, M. A.; Pugmire, D. L.; McCarroll, W. H. *J. Vac. Sci. Technol., A* **2000**, *219*, U517.
(39) Petitto, S. C.; Marsh, E. M.; Carson, G. A.; Langell, M. A. *J. Mol. Catal. A: Chem.* **2008**, *281*, 49.
(40) Marsh, E. M.; Petitto, S. C.; Harbison, G. S.; Wulser, K. W.; Langell, M. A. *J. Vac. Sci. Technol., A* **2005**, *23*, 1061.
(41) Petitto, S. C.; Langell, M. A. *J. Vac. Sci. Technol., A* **2004**, *22*, 1690.
(42) Carson, G. A.; Nassir, M. H.; Langell, M. A. *J. Vac. Sci. Technol., A* **1996**, *14*, 1637.
(43) Moulder, J. F. *Handbook of X-ray Photoelectron Spectroscopy*; Physical Electronics Division, Perkin-Elmer Corporation: Eden Prairie, MN, 1992.
(44) Shyu, J. Z.; Otto, K. *Appl. Surf. Sci.* **1988**, *32*, 246.
(45) Boyanov, B. I.; Morrison, T. I. *J. Phys. Chem.* **1996**, *100*, 16310.
(46) Yang, J. C.; Small, M. W.; Grieshaber, R. V.; Nuzzo, R. G. *Chem. Soc. Rev.* **2012**, *41*, 8179.
(47) Peuckert, M. *J. Phys. Chem.* **1985**, *89*, 2481.
(48) Ealet, B.; Gillet, E. *Surf. Sci.* **1993**, *281*, 91.
(49) Voogt, E. H.; Mens, A. J. M.; Gijzeman, O. L. J.; Geus, J. W. *Surf. Sci.* **1996**, *350*, 21.

DOI: 10.1021/acscatal.5b00842
ACS Catal. 2016, 6, 840−850